Paper

Influence of Chirped DBR Reflector on the Absorption Efficiency of Multi-nanolayer Photovoltaic Structures: Wavelength-scale Analysis by the Method of Single Expression

Hovik Baghdasaryan[1], Tamara Knyazyan[1], Tamara Hovhannisyan[1], Gurgen Mardoyan[2], Marian Marciniak[3], and Trevor Benson[4]

[1] *National Polytechnic University of Armenia, Yerevan, Armenia*
[2] *National Instruments AM LLC, Yerevan, Armenia*
[3] *National Institute of Telecommunications, Warsaw, Poland*
[4] *George Green Institute for Electromagnetics Research, Faculty of Engineering, University of Nottingham, Nottingham, UK*

https://doi.org/10.26636/jtit.2017.120117

Abstract—An electromagnetic wavelength-scale analysis of the optical characteristics of multi-nanolayer photovoltaic (PV) structures: without an antireflection coating, with an antireflection coating on the top of the structure, and with both the antireflection coating on the top and a broadband non-periodic (chirped) distributed Bragg reflector (DBR) on the bottom of the structure is performed. All the PV structures studied are based on a Si p-i-n type absorber supported by a metallic layer (Cu) and SiO_2 substrate. The top-to-bottom electromagnetic analysis is performed numerically by the method of single expression (MSE). Absorbing and reflecting characteristics of the multi-nanolayer PV structures are obtained. The influence of the thicknesses and permittivities of the layers of the PV structures on the absorbing characteristics of the structures is analyzed to reveal favourable configurations for enhancement of their absorption efficiency. The localizations of the electric component of the optical field and the power flow distribution within all the PV structures considered are obtained to confirm an enhancement of the absorption efficiency in the favorable configuration. The results of the electromagnetic wavelength-scale analysis undertaken will have scientific and practical importance for optimizing the operation of thin-film multi-nanolayer PV structures incorporating a chirped DBR reflector with regards to enhancing their efficiency.

Keywords—antireflection coating, chirped distributed Bragg reflector, electromagnetic modeling, method of single expression, multi-nanolayer photovoltaic structure, photovoltaics.

1. Introduction

Today's photovoltaic (PV) technology is one of the most attractive, scalable and mature renewable energy sources. PV technology has gained great scientific and practical interest since the end of the 19-th century and now is proven as the cleanest and safest of all energy technologies. Due to growing demand for renewable energy sources, the manufacturing of solar cells and photovoltaic arrays has advanced considerably in recent years [1]–[5].

Photovoltaics are based on the photovoltaic effect by which solar energy is converted directly into electrical energy by photovoltaic or solar cells. The conversion efficiency of a PV cell depends on the probability of absorption of an incident photon, generating an electron-hole pair, which can contribute to the external electric current.

Though today's PVs technology is well developed, and has been extensively exploited for household and industrial applications, there is still a need to enhance the PV efficiency over a wider spectral range, whilst using a cheap material base and a low cost technology for the mass production of durable PV devices.

Materials used for the first generation of PV cells included monocrystalline and polycrystalline silicon, for the second generation of PV cells cadmium telluride, copper indium gallium selenide/sulfide, and thin films from amorphous silicon were used. The third generation of PV cells uses different organic polymers, perovskite crystals, monocrystalline and polycrystalline graphene, quantum dots, and multilayers of different semiconductor materials.

Nowadays PV cells are thin-film cells with absorbing layer thicknesses that are of the same order or smaller than the operating wavelength [5], [6]. Thin films essentially reduce the amount of semiconductor material required for each PV cell compared to bulk PV cells and hence lower the cost of production [2], [7]. The probability of photon absorption increases with an increased thickness of the absorbing layer [8]. However, enhancement of the recombination probability decreases the probability of conversion of absorbed photons into electrical current as the

active layer thickness increases. For better light harvesting in PV cells different multilayer optical structures are used. Generally, they consist of an absorbing layer covered from top and bottom, correspondingly by transparent and reflecting metal electrodes. Some structures have an antireflection coating above the top transparent electrode to reduce reflection losses in the PV cell [9], [10]. Antireflection coatings can improve the absorption efficiency when the thickness of an absorbing layer much greater than the operating wavelength. When the thickness of the absorbing layer is comparable to or smaller than the operating wavelength high-reflectivity dielectric mirrors are used to enhance the absorption over a narrow spectral and angular range. The dielectric mirrors are usually high reflectivity distributed Bragg reflectors (DBRs) [11]–[13]. DBRs should exhibit a high reflectivity in the spectral range where the absorption of the PV cell is weak to enhance absorption, and a low reflectivity where the absorption of the PV cell is strong. DBRs made as non-periodic dielectric stacks, where the thicknesses of bilayers are monotonously changed by some linear, quadratic, exponential or other law, are called chirped DBRs. Absorption in thin-film PV cells using chirped DBR mirrors can be enhanced over a wider spectral range by providing higher efficiency in comparison with those using conventional reflectors [7], [14]–[16]. By tailoring the law of chirp, and the number and thickness of bilayers in chirped DBRs, the efficiency of such PV cells can essentially be enhanced.

It is important to note that for the analysis of a PV cell's efficiency enhancement there is a need to apply two different methodologies: the first is optical (electromagnetic) modeling directed to light-matter interaction analysis and the second is an analysis of the physics of semiconductors and semiconductor junctions. The optical analysis is the less investigated topic for thin-film nano-scale PV structures. Semiconductor junction physics has been intensively analyzed and is a well-established area. There is a need for detailed optical simulations to understand and further optimize the beneficial effects of the PV cells [15].

The present paper is devoted to the wavelength-scale numerical analysis, by the method of single expression (MSE) [13], [17]–[21], of the optical characteristics of multi-nanolayer PV structures:

- without an antireflection coating,
- with an antireflection coating on the top of the structure,
- with both an antireflection coating on the top and chirped DBRs on the bottom of the structure.

The influence of layer thicknesses and permittivities on the optical characteristics of multi-nanolayer PV cells is analyzed by observing the localization of the electric component of the optical field and the power flow density distribution within the structures. The numerical modeling reveals an optimal PV structure for efficient light absorption.

2. Modeling Method

The modeling has been performed by the method of single expression (MSE) which is a convenient and correct tool for wavelength-scale analysis of multilayer and modulated structures comprising dielectric, semiconductor or metallic layers in the presence of loss, gain or (Kerr-type) nonlinearity [13], [17]–[21].

Here the backbone of the MSE for wave normal incidence on a non-magnetic multilayer structure is presented. From Maxwell's equations in 1D case the following Helmholtz equation can be obtained for linearly polarized complex electric field component $\dot{E}_x(z)$:

$$\frac{d^2\dot{E}_x(z)}{dz^2} + k_0^2\dot{\varepsilon}(z)\dot{E}_x(z) = 0\,, \tag{1}$$

where $k_0 = \frac{\omega}{c}$ is the free space propagation constant, $\dot{\varepsilon}(z) = \varepsilon'(z) + i\varepsilon''(z)$ is the complex relative permittivity of a medium. The essence of the MSE is the presentation of a general solution of Helmholtz equation for the electric field component $\dot{E}_x(z)$ in the special form of a single expression:

$$\dot{E}_x(z) = U(z)\cdot \mathrm{e}^{-iS(z)} \tag{2}$$

instead of the traditional presentation as a sum of counter-propagating waves. Here $U(z)$ and $S(z)$ are real quantities describing the resulting electric field amplitude and phase, respectively. A time dependence of $\mathrm{e}^{i\omega t}$ is assumed, but suppressed, throughout the analysis. A solution in the form (2) prevails upon the traditional approach of counter-propagating waves and is more general because it does not rely on the superposition principle. This form of solution describes all possible distributions in space of electric field amplitude, corresponding to propagating, standing or evanescent waves. It means that no preliminary assumptions concerning the solution of the Helmholtz equation in different media are needed in the MSE. This gives advantages in allowing investigation of the interaction of a wave with any longitudinally non-uniform linear and intensity dependent non-linear media with the same ease and exactness.

Based on expression (2) the Helmholtz equation (1) is reformulated to the set of first order differential equations regarding the electric field amplitude $U(z)$, its spatial derivative $Y(z)$ and a quantity $P(z)$ proportional to the power flow density (Poynting vector) in a medium:

$$\begin{cases} \dfrac{dU(z)}{d(k_0z)} = Y(z) \\ \dfrac{dY(z)}{d(k_0z)} = \dfrac{P^2(z)}{U^3(z)} - \varepsilon'(z)\cdot U(z) \\ \dfrac{dP(z)}{d(k_0z)} = \varepsilon''(z)\cdot U^2(z) \end{cases}, \tag{3}$$

where $P(z) = U^2(z)\frac{dS(z)}{d(k_0z)}$. An actual value of Poynting vector can be obtained by multiplication of $P(z)$ by $\frac{1}{2}\sqrt{\frac{\varepsilon_0}{\mu_0}}$, where ε_0 and μ_0 are free space permittivity and permeability, respectively. Hereafter this multiplier is suppressed.

The sign of $\varepsilon'(z)$ can be taken either positive or negative describing relevant electromagnetic features of dielectric or metal (plasma), correspondingly. The sign of $\varepsilon''(z)$ indicates loss or gain in a medium.

The set of differential equations (3) is integrated numerically starting from the non-illuminated side of a multilayer structure, where only one outgoing traveling wave is supposed. Initial values for the integration are obtained from the boundary conditions of electrodynamics at the non-illuminated side of the structure (at $z = L$): $U(L) = E_{tr}$, $Y(L) = 0$ and $P(L) = \sqrt{\varepsilon_r} E_{tr}^2 = P_{tr}$, where P_{tr} is proportional to the Poynting vector in the medium beyond the structure (at $z > L$) of relative permittivity ε_r, and E_{tr} is the amplitude of the transmitted wave.

Numerical integration of the set (3) goes step by step towards the illuminated side of the structure taking into account the actual value of the structure's relative permittivity for the given coordinate at each step of the integration. In the process of integration it is possible to record any variable of the set (3) in order to have full information regarding distributions of electric field amplitude, its derivative and power flow density inside and outside of a structure. At the borders between the layers constituting a multilayer structure, the ordinary boundary conditions of electrodynamics bring continuity of $U(z)$, $Y(z)$ and $P(z)$. From the boundary conditions of electrodynamics at the illuminated side of the structure the amplitude of incident wave E_{inc}

$$E_{inc} = \left| \frac{U^2(0) \cdot \sqrt{\varepsilon_l} + P(0) + iU(0) \cdot Y(0)}{2U(0) \cdot \sqrt{\varepsilon_l}} \right|, \qquad (4)$$

and the power reflection coefficient R

$$R = \left| \frac{E_{ref}}{E_{inc}} \right|^2 = \left| \frac{U^2(0) \cdot \sqrt{\varepsilon_l} - P(0) - iU(0) \cdot Y(0)}{U^2(0) \cdot \sqrt{\varepsilon_l} + P(0) + iU(0) \cdot Y(0)} \right|^2, \qquad (5)$$

are restored at the end of the calculation. Here $U(0)$ is the resultant amplitude of the electromagnetic wave, $Y(0)$ is its derivative and $P(0)$ is proportional to the power flow density at the illuminated interface of the structure at $z = 0$, E_{ref} is the amplitude of the reflected wave, ε_l is the relative permittivity of the medium in front of the structure, at $z < 0$, and in the considered case is air $\varepsilon_l = 1$. In accordance with the energy conservation law $P(0) = P_{inc} - P_{ref}$, where $P_{inc} = \sqrt{\varepsilon_l} \cdot E_{inc}^2$ is proportional to the incident power flow density and $P_{ref} = \sqrt{\varepsilon_l} \cdot E_{ref}^2$ is proportional to the reflected power flow density. The power transmission coefficient $T = \frac{P_{tr}}{P_{inc}} = \frac{\sqrt{\varepsilon_r} E_{tr}^2}{\sqrt{\varepsilon_l} E_{inc}^2}$ is defined as the ratio of the transmitted power flow density P_{tr} to the incident one P_{inc}.

3. Numerical Analysis of Multi-Nanolayer Photovoltaic Structures

In the current paper the PV structures of the following configurations: a) without antireflection coating, b) with an antireflection coating on the top of the PV structure, and c) both the antireflection coating on the top and a broadband non-periodic (chirped) distributed Bragg reflector (DBR) on the bottom of the PV structure, are considered. All PV structures are based on a Si p-i-n type absorber and supported by a metallic mirror (Cu) and SiO_2 substrate.

The results of a preliminary analysis of the thin-film multi-nanolayer PV structure with chirped DBR on the top of the structure was presented at ICTON 2016 [22].

Chirped DBR mirrors should possess broadband reflective features in the range of 350–750 nm in the vicinity of the central wavelength of 550 nm of the sun's maximal radiation.

The consideration and analysis of the PV structures is aiming to reveal an optimal structure for efficient absorption of incident light in the specific region of the PV structure, namely in the "i" region of the p-i-n junction, where generation of electron-hole pairs is favorable.

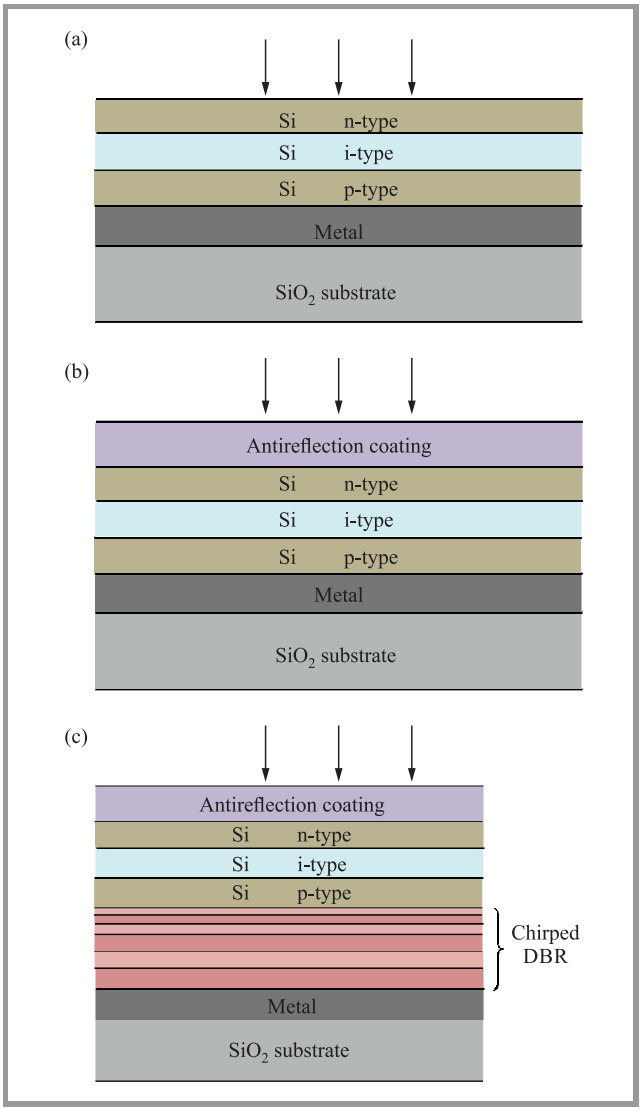

Fig. 1. Schematic representations of the PV structures: (a) without antireflection coating, (b) with an antireflection coating on the top of the PV structure, and (c) with both the antireflection coating on the top and a chirped DBR on the bottom of the PV structure.

The schematic representations of the considered PV structures are shown in Figs. 1a–1c, respectively.

In the structures considered the thickness of the substrate of relative permittivity $\varepsilon_{SiO_2} = 2.1313$ is taken to be $L_{SiO_2} = 100\ \mu$m. The thickness of the metallic layer, of relative permittivity $\varepsilon_m = \varepsilon'_m - \varepsilon''_m = -6.12 - i4.48$ at the central wavelength of $\lambda_0 = 550$ nm, is taken as $L_m = 0.6\ \mu$m. Dispersive properties of Cu in the range of wavelengths 350–750 nm are taken into account [23]. Dispersion of other materials of the structure are not taken into account.

The p-i-n absorbing region made of silicon (Si) has the following parameters: *p*-type and *n*-type layers of relative permittivity $\varepsilon_n = \varepsilon_p = 15$ have thicknesses $L_p = 1.45$ *mu*m and $L_n = 0.255\ \mu$m, respectively. The *i*-type layer of relative permittivity $\varepsilon_i = \varepsilon'_i - i\varepsilon''_i = 15.5 - i0.3$ has a thickness of $L_i = 1\ \mu$m.

The antireflection coating made of TiO_2 of relative permittivity $\varepsilon_{coat} = 5$ has the thickness $L_{coat} = 61.5$ nm.

Chirped DBRs made of TiO_2 are composed of 7 bilayers of slightly different high $\varepsilon_{H-TiO_2} = 5$ and low $\varepsilon_{L-TiO_2} = 3.5$ relative permittivities. The permittivity of a material can be lowered by introducing porosity, provided that the pore sizes are much smaller than the electromagnetic wavelengths of interest [24]. The thicknesses of the layers of high and low permittivities decrease gradually towards the illuminated side of the structure to provide a chirp law for the DBR. The thicknesses of the layers of low permittivity are as follows (starting from the bottom of the structure): $L_{L1-TiO_2} = 108$ nm, $L_{L2-TiO_2} = 1038$ nm, $L_{L3-TiO_2} = 97$ nm, $L_{L4-TiO_2} = 91$ nm, $L_{L5-TiO_2} = 85$ nm, $L_{L6-TiO_2} = 79$ nm, $L_{L7-TiO_2} = 73$ nm.

The thicknesses of the layers of high permittivity are as follows (starting from the bottom of the structure): $L_{H1-TiO_2} = 91$ nm, $L_{H2-TiO_2} = 86$ nm, $L_{H3-TiO_2} = 81$ nm, $L_{H4-TiO_2} = 76$ nm, $L_{H5-TiO_2} = 71$ nm, $L_{H6-TiO_2} = 66$ nm, $L_{H7-TiO_2} = 61$ nm.

The results of modeling of the PV structures considered are presented below successively in following subsections.

3.1. The Modeling of the PV Structure without an Antireflection Coating

The reflection spectrum of the PV structure without an antireflection coating (Fig. 1a) with the above-mentioned parameters is presented in Fig. 2 for the range of the incident wavelengths λ_0 = 350–750 nm.

As it follows from Fig. 2 the reflection spectrum of the PV structure without antireflection coating has an oscillating character with maxima and minima at specific wavelengths. The oscillations of the reflectance in the considered frequency range are stipulated by an optical wave resonant interaction with the wavelength-scaled multilayer dielectric-semiconductor-metal structure.

In order to understand which part of the incident light is absorbed in the i absorbing layer of p-i-n region contributing to the PV effect it is useful to analyse the distributions

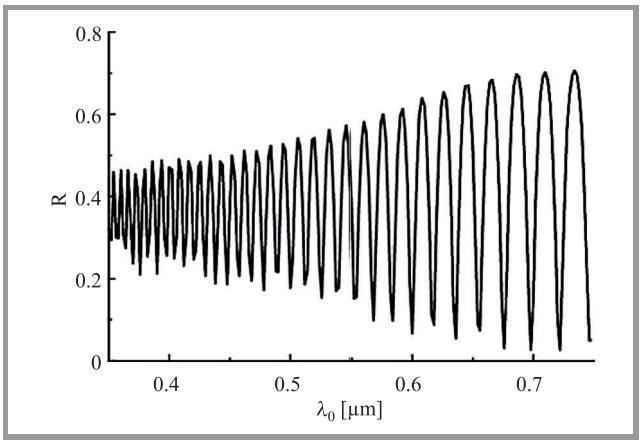

Fig. 2. The reflection spectrum of the PV structure without antireflection coating (presented in Fig. 1a).

of the electric component of optical field and the power flow density within and outside of the structure. The permittivity profile of the PV structure without antireflection coating and the distributions of the electric component of the optical field and the power flow density within and outside of the structure at the central wavelength λ_0 = 550 nm, corresponding to the sun's maximal radiation, are presented in Fig. 3.

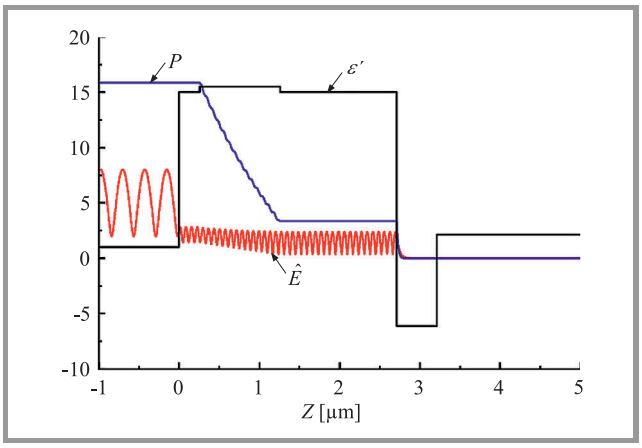

Fig. 3. The relative permittivity profile ε' of the PV structure without antireflection coating (presented in Fig. 1a) and the distributions of electric field amplitude $\hat{E}$ and power flow density *P* within and outside of the structure at the wavelength λ_0 = 550 nm, $P_{inc} = 25$ a.u., the reflectance $R = 0.366$.

As can be seen from Fig. 3, electric field amplitude has an oscillating character in the p-i-n region and forms a standing wave pattern in the front of the structure (at $z < 0$) due to some reflection from it. A decrease of power flow density in the *i* absorbing layer of $\Delta P_{p-i-n} = 12.5135$ a.u. is observed, indicating an absorption rate $\frac{\Delta P_{p-i-n}}{P_{inc}} \approx 0.5$ (about 50%) of the incident light ($P_{inc} = 25$ a.u.) contributing to the PV effect. Outside of the absorbing region the power flow density is constant except for some decay within the metallic layer ($\Delta P_m = 3.3485$ a.u.). The absorption rate $\frac{\Delta P_m}{P_{mc}} \approx 0.134$ in the metal is about 13.4%. Thus,

essential absorption of the incident energy takes place in the "i" absorbing layer of the structure. The rest of the incident energy, 36.6%, relates to the reflectance from the structure.

3.2. The Modeling of the PV Structure with an Antireflection Coating on the Top of the Structure

The reflection spectrum of the PV structure with the antireflection coating on the top of the structure (Fig. 1b) with above-mentioned parameters is presented in Fig. 4 for the range of incident wavelengths λ_0 = 350–750 nm.

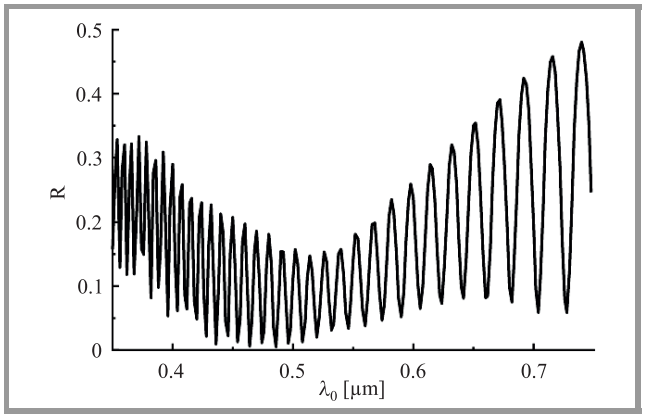

Fig. 4. The reflection spectrum of the PV structure with the antireflection coating on the top of the structure (presented in Fig. 1b).

It follows from Fig. 4 that the reflection spectrum of the PV structure with the antireflection coating also has an oscillating character, however the average value of the reflectance oscillations has a minimum around $\lambda_0 = 500$ nm.

As with the previous structure it is useful to analyse the distributions of the electric component of the optical field and the power flow density within the considered structure. The permittivity profile of the PV structure with the antireflection coating on the top of the structure and the distributions of electric component of optical field and power flow density within the structure at the central wavelength $\lambda_0 = 550$ nm of the sun's maximal radiation are presented in Fig. 5.

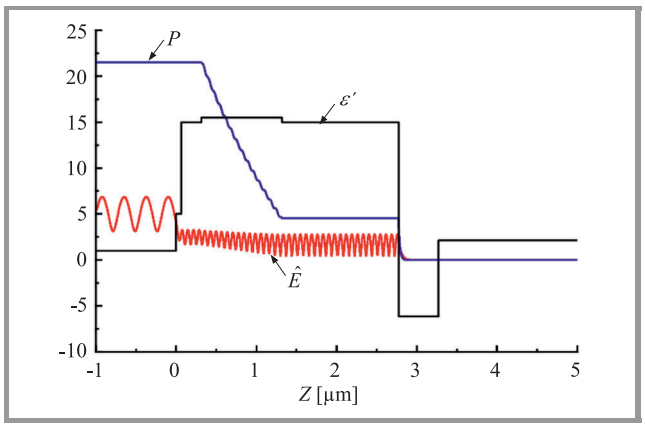

Fig. 5. The relative permittivity profile ε' of the PV structure with antireflection coating on the top of the structure (presented in Fig. 1b) and the distributions of electric field amplitude $\hat{E}$ and power flow density P within the structure at the wavelength λ_0 = 550 nm, $P_{inc} = 25$ a.u., the reflectance $R = 0.14$.

As can be seen from Fig. 5, the electric field amplitude has an oscillating character in the p-i-n region and forms a standing wave pattern in front of the structure (at $z < 0$) due to some reflection from the structure. A decrease of power flow density in the "i" absorbing layer $\Delta P_{p-i-n} = 16.97$ a.u. is observed, indicating an absorption rate $\frac{\Delta P_{p-i-n}}{P_{inc}} \approx 0.679$ (about 68%) of the incident light ($P_{inc} =$ 25 a.u.) contributing to the PV effect. Outside of this region the power flow density is constant except for some decay within the metallic layer ($\Delta P_m = 4.541$ a.u.). The absorption rate $\frac{\Delta P_m}{P_{inc}} \approx 0.182$ nm in the metal is about 18%. Thus, essential absorption of incident energy takes place in the "i" absorbing layer of the structure. The rest of the incident energy, 14%, relates to the reflectance from the structure.

3.3. The Modeling of the PV Structure with an Antireflection Coating on the Top and a Chirped DBR on the Bottom of the Structure

The reflectance of the PV structure with the antireflection coating on the top and the chirped DBR on the bottom of the PV structure (Fig. 1c) with above-mentioned parameters is presented in Fig. 6 for the range of incident wavelengths λ_0 = 350–750 nm.

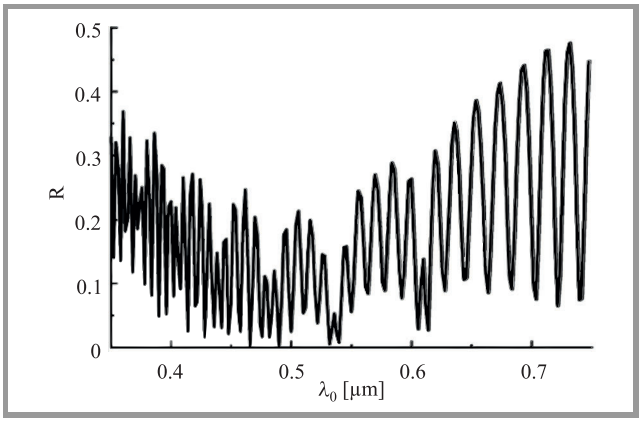

Fig. 6. The reflection spectrum of the PV structure with the antireflection coating on the top and the chirped DBR on the bottom of the structure (presented in Fig. 1c).

It follows from Fig. 6 that the reflection spectrum of the PV structure with the antireflection coating on the top and the chirped DBR on the bottom of the structure also has an oscillating character with maxima and minima at specific wavelengths. However, the average value of the reflectance oscillations has a minimum around $\lambda_0 = 550$ nm.

As with the previous structures it is useful to analyse the distributions of the electric component of the optical field and the power flow density within and outside of the struc-

ture considered. The relative permittivity profile of the PV structure with the antireflection coating on the top and the chirped DBR on the bottom of the structure, and the distributions of the electric component of the optical field and the power flow density within the structure, are presented in Fig. 7 for the central wavelength $\lambda_0 = 550$ nm of the sun's maximal radiation.

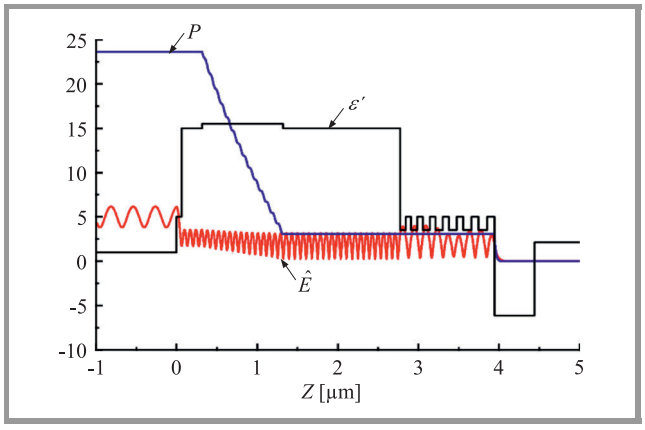

Fig. 7. The relative permittivity profile ε' of the PV structure with the antireflection coating on the top and the chirped DBR on the bottom of the structure (presented in Fig. 1c) and the distributions of electric field amplitude $\hat{E}$ and power flow density P within the structure at the wavelength $\lambda_0 = 550$ nm, $P_{inc} = 25$ a.u., the reflectance $R = 0.056$.

As can be seen from Fig. 7, the electric field amplitude has an oscillating character in the p-i-n region and forms a standing wave pattern in front of the structure (at $z < 0$) due to some reflection from the structure. A strong decrease of power flow density in the "i" absorbing layer $\Delta P_{p-i-n} = 20.52$ a.u. is observed, indicating an absorption rate $\frac{\Delta P_{p-i-n}}{P_{inc}} \approx 0.8208$ (about 82.1%) of incident light ($P_{inc} = 25$ a.u.) contributing to the PV effect. Outside of this region the power flow density is constant except for the small decay within the metallic layer ($\Delta P_m = 3.08$ a.u.). The absorption rate $\frac{\Delta P_m}{P_{inc}} \approx 0.1232$ in the metal is about 12.3%. Thus, essential absorption of incident energy takes place in the i absorbing layer of the structure. The rest of the incident energy, 5.6%, relates to the reflectance from the structure as can be seen from Fig. 6.

The results of comparative analysis of the considered PV structures are summarized and presented in Table 1.

Table 1
Example results of the new metric

Structure described in	$R = \frac{P_{ref}}{P_{inc}}$	$\frac{\Delta P_{p-i-n}}{P_{inc}}$	$\frac{\Delta P_m}{P_{inc}}$
3.1	≈ 0.366	≈ 0.5	≈ 0.134
3.2	≈ 0.14	≈ 0.679	≈ 0.181
3.3	≈ 0.056	≈ 0.821	≈ 0.123

It is evident that the structure with the antireflection coating on the top and the broadband non-periodic (chirped) DBR reflector on the bottom of the PV structure is favorable for light absorption in the i region of the p-i-n structure.

4. Conclusions

An electromagnetic wavelength-scale numerical analysis of the optical characteristics of thin-film multi-nanolayer PV structures has been performed by the MSE. The following configurations of the PV structures are considered: without an antireflection coating, with an antireflection coating on the top of the structure, and with both the antireflection coating on the top and a broadband non-periodic (chirped) distributed Bragg reflector (DBR) on the bottom of the structure. All PV structures are based on a Si p-i-n type absorber supported by a metallic layer (Cu) and SiO_2 substrate.

The reflection spectra of all structures have an oscillating character in the whole spectral range of λ_0 = 350–750 nm nm with maxima and minima at specific wavelengths. The oscillations in the frequency range considered are stipulated by an optical wave resonant interaction with the wavelength-scaled multilayer dielectric-semiconductor-metal structures. At the fixed wavelength $\lambda_0 = 550$ nm (the wavelength of the sun's maximal radiation and the central part of the spectrum considered) the distributions of electric field amplitude and power flow density within and outside of the structures are obtained. For all structures high absorption of incident light is observed in the i-layer of the p-i-n junction. The highest absorption of incident light takes place in the i-layer of the p-i-n junction of the structure with the antireflection coating on the top and the broadband non-periodic (chirped) DBR reflector on the bottom of the PV structure while the lowest absorption in the metallic layer is observed. Thus, this structure is favorable for strong absorption of the incident light that will contribute to the PV effect.

Though the current analysis is performed for a plane wave normal incidence on the PV structures, the MSE permits the case of an oblique incidence of a plane wave to be considered as well [25].

Acknowledgement

This work was supported by the RA MES State Committee of Science, in the frame of the research project no. 15T-2J372.

References

[1] G. K. Singh, "Solar power generation by PV (photovoltaic) technology: A review", *Energy*, vol. 53, pp. 1–13, 2013.

[2] B. Parida, S. Iniyan, and R. Goic, "A review of solar photovoltaic technologies", *Renewable and Sustain. Energy Rev.*, vol. 15, no. 3, pp. 1625–1636, 2011.

[3] M. A. Green, K. Emery, Y. Hishikawa, W. Warta, and E. D. Dunlop, "Solar cell efficiency tables (Version 45)", *Progr. in Photovolt: Res. and Appl.*, vol. 23, no. 1, pp. 1–9, 2015 (doi: 10.1002/pip.2573).

[4] R. W. Miles, K. M. Hynes, and I. Forbes, "Photovoltaic solar cells: An overview of state-of-the-art cell development and environmental issues", *Progr. in Crystal Growth and Charact. of Mater.*, vol. 51, no. 1–3, pp. 1–42, 2005.

[5] Y. Hamakawa, Ed., *Thin-Film Solar Cells: Next Generation Photovoltaics and Its Applications*. Springer, 2004.

[6] A. G. Aberle, "Thin-film solar cells", *Thin Solid Films*, vol. 517, no. 17, pp. 4706–4710, 2009.

[7] I. J. Kuzma-Filipek, F. Duerinckx, E. Van Kerschaver, K. Van Nieuwenhuysen, G. Beaucarne, and J. Poortmans, "Chirped porous silicon reflectors for thin-film epitaxial silicon solar cells", *J. of Appl. Phys.*, vol. 104, no. 7, pp. 073529-1–073529-8, 2008 (doi: 10.1063/1.2993753).

[8] T. Tiedje, E. Yablonovitch, G. D. Cody, and B. G. Brooks, "Limiting efficiency of silicon solar cells", *IEEE Trans. Electron Devices*, vol. ED-31, no. 5, pp. 711–716, 1984.

[9] J. Zhao and M. A. Green, "Optimized antireflection coatings for high-efficiency silicon solar cells", *IEEE Trans. Electron Devices*, vol. 38, no. 8, pp. 1925–1934, 1991.

[10] J. K. Selj, D. Young, and S. Grover, "Optimization of the antireflection coating of thin epitaxial crystalline silicon solar cells", *Energy Procedia*, vol. 77, pp. 248–252, 2015.

[11] P. Yeh, *Optical Waves in Layered Media*. N.Y.: Willey, 1988.

[12] D. I. Babic and S. W. Corzine, "Analytic expressions for the reflection delay, penetration depth, and absorptance of quarter-wave dielectric mirrors", *IEEE J. Quantum Elect.*, vol. 28, pp. 514–524, 1992.

[13] H. V. Baghdasaryan, T. M. Knyazyan, T. H. Baghdasaryan, B. Witzigmann, and F. Roemer, "Absorption loss influence on optical characteristics of multilayer distributed Bragg reflector: wavelength-scale analysis by the method of single expression", *Opto-Electron. Rev.*, vol. 18, no. 4, pp. 438–445, 2010 (doi: 10.2478/s11772-010-0049-0).

[14] M. Agrawal and P. Peumans, "Broadband optical absorption enhancement through coherent light trapping in thin-film photovoltaic cells", *Optics Express*, vol. 16, no. 8, pp. 5385–5396, 2008 (doi: 10.1364/OE.16.005385).

[15] F. Duerinckx *et al.*, "Simulation and implementation of a porous silicon reflector for epitaxial silicon solar cells", *Progr. in Photovolt: Res. and Appl.*, vol. 16, pp. 399–407, 2008.

[16] J. Zheng, R. A. Barton, and D. Englund, "Broadband coherent absorption in chirped-planar-dielectric cavities for 2D-material-based photovoltaics and photodetectors", *ACS Photonics*, vol. 1, no. 9, pp. 768–774, 2014 (doi: 10.1021/ph500107b).

[17] H. V. Baghdasaryan, "Method of backward calculation", in *Photonic Devices for Telecommunications: How to Model and Measure*, G. Guekos, Ed. Springer, 1999, pp. 56–65.

[18] H. V. Baghdasaryan and T. M. Knyazyan, "Problem of plane EM wave self-action in multilayer structure: An exact solution", *Optical and Quant. Electron.*, vol. 31, no. 9, pp. 1059–1072, 1999 (doi: 10.1023/A:1007024312874).

[19] H. V. Baghdasaryan and T. M. Knyazyan, "Modelling of strongly nonlinear sinusoidal Bragg gratings by the Method of Single Expression", *Optical and Quant. Electron.*, vol. 32, no. 6-8, pp. 869–883, 2000.

[20] H. V. Baghdasaryan, T. M. Knyazyan, T. H. Baghdasaryan, B. Witzigmann, and F. Roemer, "Absorption loss influence on optical characteristics of multilayer distributed Bragg reflector: wavelength-scale analysis by the method of single expression", *Opto-Electron. Rev.*, vol.18, pp. 438–445, 2010.

[21] H. V. Baghdasaryan, *Basics of the Method of Single Expression: New Approach for Solving Boundary Problems in Classical Electrodynamics*. Yerevan: Chartaraget, 2013.

[22] H. V. Baghdasaryan, T. M. Knyazyan, T. T. Hovhannisyan, G. R. Mardoyan, and M. Marciniak, "Wavelength-scale analysis of influence of chirped DBRs on optical characteristics of multi-nanolayer Photovoltaic Cells", in *Proc. of 18th In. Conf. on Transp. Opt. Netw. ICTON 2016*, Trento, Italy, 2016, We.P.33, 5 pages.

[23] E. D. Palik, Ed., *Handbook of Optical Constants of Solids.* Academic Press, 1998.

[24] A. Vincent, S. Babu, E. Brinley, A. Karakoti, S. Deshpande, and S. Seal, "Role of catalyst on refractive index tenability of porous silica antireflective coatings by sol-gel technique", *J. Phys. Chem. C*, vol. 111, no. 23, pp. 8291–8298, 2007.

[25] H. V. Baghdasaryan, T. M. Knyazyan, T. H. Baghdasaryan, and G. G. Eyramjyan, "Development of the Method of Single Expression (MSE) for analysis of plane wave oblique incidence on multilayer structures having complex permittivity and permeability", in *Proc. of 10th Int. Conf. on Transp. Opt. Netw. ICTON 2008*, Athens, Greece, 2008, Th.A1.4, pp. 250–254.

Gurgen R. Mardoyan graduated in Radio-engineering from the State Engineering University of Armenia (now National Polytechnic University of Armenia, NPUA) in 2010. He received M.Sc. degree in Radio-engineering and Communications in 2012 and the Ph.D. degree in Wireless Communications in 2015 from National Polytechnic University of Armenia. His postgraduate research dealt with problems of spectrum efficiency in MIMO communication systems, while multiple channels in both transmitters and receivers were not fully phase-coherent. Since 2010 he works at National Instruments as a Systems Engineer prototyping RF systems for wireless/cellular test, RF component test, radio-navigation, Radars and next generation wireless communications. Since 2016 he focuses on Advanced Driver Assistance Systems (ADAS), particularly on 77 GHz automotive radar test applications. Collaborating with R&D department of National Instruments he is working on software development for automotive radar test systems and actively participating in engagements with end-users worldwide.

E-mail: gurgen.mardoyan@gmail.com
National Instruments AM LLC
123 Hovsep-Emin St
EIF Entrance, 0051 Yerevan, Armenia

Trevor M. Benson received a First Class honours degree in Physics and the Clark Prize in Experimental Physics from the University of Sheffield in 1979, a Ph.D. in Electronic and Electrical Engineering from the same University in 1982 and the D.Sc. degree from the University of Nottingham in 2005.

After spending over six years as a Lecturer at University College Cardiff, he moved to The University of Nottingham in 1989. He was promoted to a Chair in Optoelectronics in 1996, having previously been Senior Lecturer (1989) and Reader (1994). Professor Benson's research interests include experimental and numerical studies of electromagnetic fields and waves with particular emphasis on the theory, modeling and simulation of optical waveguides, lasers and amplifiers, nano-scale photonic circuits and sensors, and electromagnetic compatibility. He is a Fellow of the Institute of Engineering Technology (FIET) and the Institute of Physics (FInst.P). He was elected a Fellow of the Royal Academy of Engineering in 2005 for his achievements in the development of versatile design software used to analyze propagation in optoelectronic waveguides and photonic integrated circuits.

E-mail: trevor.benson@nottingham.ac.uk
George Green Institute for Electromagnetics Research
Faculty of Engineering
University of Nottingham
University Park
Nottingham NG7 2RD, UK

Hovik V. Baghdasaryan – for biography, see this issue, p. 34.

Marian Marciniak, Tamara M. Knyazyan, Tamara T. Hovhannisyan – for biographies, see this issue, p. 35.